



NRL/MR/6793--96-7788

Initial Operation of a High Power, Frequency-Doubling X-Band Magnicon Amplifier

S.H. GOLD
A.W. FLIFLET

*Beam Physics Branch
Plasma Physics Division*

W.M. MANHEIMER
*Senior Scientist for Fundamental Plasma Processes
Plasma Physics Division*

A.K. KINKEAD
*Sachs/Freeman Associates
Landover, MD*

B. HAFZI
*Icarus Research
Bethesda, MD*

January 18, 1996

19960228 109

DTIC QUALITY INSPECTED 1

Approved for public release; distribution unlimited.

REPORT DOCUMENTATION PAGE

Form Approved
OMB No. 0704-0188

Public reporting burden for this collection of information is estimated to average 1 hour per response, including the time for reviewing instructions, searching existing data sources, gathering and maintaining the data needed, and completing and reviewing the collection of information. Send comments regarding this burden estimate or any other aspect of this collection of information, including suggestions for reducing this burden, to Washington Headquarters Services, Directorate for Information Operations and Reports, 1215 Jefferson Davis Highway, Suite 1204, Arlington, VA 22202-4302, and to the Office of Management and Budget, Paperwork Reduction Project (0704-0188), Washington, DC 20503.

1. AGENCY USE ONLY (Leave Blank)		2. REPORT DATE January 18, 1996	3. REPORT TYPE AND DATES COVERED Interim	
4. TITLE AND SUBTITLE Initial Operation of a High Power, Frequency-Doubling X-Band Magnicon Amplifier			5. FUNDING NUMBERS PE - 67-3788-05	
6. AUTHOR(S) S.H. Gold, A.K. Kinkead,* A.W. Fliflet, B. Hafizi,† and W.M. Manheimer				
7. PERFORMING ORGANIZATION NAME(S) AND ADDRESS(ES) Naval Research Laboratory Washington, DC 20375-5320			8. PERFORMING ORGANIZATION REPORT NUMBER NRL/MR/6793-96-7788	
9. SPONSORING/MONITORING AGENCY NAME(S) AND ADDRESS(ES) Office of Naval Research 800 North Quincy Street Arlington, VA 22217-5660			10. SPONSORING/MONITORING AGENCY REPORT NUMBER U.S. Department of Energy Washington, DC 20585	
11. SUPPLEMENTARY NOTES *Sachs/Freeman Associates, Inc., 1401 McCormick Dr., Landover, MD 20785 †Icarus Research, PO Box 30780, Bethesda, MD 20824				
12a. DISTRIBUTION/AVAILABILITY STATEMENT Approved for public release; distribution unlimited.			12b. DISTRIBUTION CODE A	
13. ABSTRACT (Maximum 200 words) This paper reports the initial high power operation of a frequency-doubling magnicon amplifier at 11.120 GHz. The deflection cavities operate at 5.560 GHz. The device is operating in a single-pulse mode at 650 kV and ~225 A, using a 5.5-mm-diam. beam from a plasma cathode, at a magnetic field of 6.7-8.2 kG. In order to overcome a gain saturation problem in the deflection cavities caused by plasma loading, the penultimate deflection cavity is operated very close to self-oscillation. The typical output pulse length is 100 nsec FWHM, and is limited by rf breakdown of the penultimate cavity. Based on the measured far-field antenna pattern and absolute calibration of all microwave components, the measured output power is 14 MW (± 3 dB), corresponding to an efficiency of ~10%.				
14. SUBJECT TERMS Magnicon Microwave amplifier Second harmonic			15. NUMBER OF PAGES 37	
17. SECURITY CLASSIFICATION OF REPORT UNCLASSIFIED			16. PRICE CODE	
18. SECURITY CLASSIFICATION OF THIS PAGE UNCLASSIFIED		19. SECURITY CLASSIFICATION OF ABSTRACT UNCLASSIFIED		20. LIMITATION OF ABSTRACT UL

CONTENTS

I. INTRODUCTION	1
II. APPARATUS	2
III. PRELIMINARY EXPERIMENTS	4
IV. HIGH POWER EXPERIMENTS	5
A. HETERODYNE MEASUREMENTS	6
B. FAR-FIELD MEASUREMENTS	8
C. SIMULATIONS	10
V. SUMMARY AND CONCLUSIONS	15
ACKNOWLEDGMENTS	17
REFERENCES	18

INITIAL OPERATION OF A HIGH POWER, FREQUENCY-DOUBLING X-BAND MAGNICON AMPLIFIER

I. INTRODUCTION

The magnicon [1-3] is a scanning-beam microwave amplifier that is under consideration as an alternative to klystrons for powering future high-gradient electron linear accelerators. In it, an initially linear ($v_{\perp} \sim 0$) electron beam is spun up to high transverse momentum ($\alpha \equiv v_{\perp}/v_z \sim 1$, where v_{\perp} and v_z are the perpendicular and parallel electron velocity components with respect to the axial magnetic field B) in a series of deflection cavities, the first externally driven, and then spun down again in the output cavity to generate high power radiation. All of the cavities employ synchronously rotating rf modes, the TM_{110} mode in the deflection cavities, and the TM_{210} mode in the output cavity for a device operating at the second harmonic of the drive frequency. Since the electron deflection is produced by these synchronously rotating modes, the instantaneous position of the beam centroid and the sense of electron gyration vary in synchronism with the rf in each of the deflection cavities as well as in the output cavity. This synchronism makes possible a highly efficient interaction in the output cavity. The potential for high power at high efficiency in a high gain, highly phase stable amplifier tube makes the magnicon an attractive candidate to replace klystrons in future linear accelerators operating at frequencies above 10 GHz.

We have previously published a design for a 50 MW, 50% efficient frequency-doubling X-band magnicon amplifier, using a 500 kV, 172 A electron beam [4]. This design requires the use of a 2-mm-diam. electron beam, such as might be produced from the best high-convergence thermionic electron guns [5]. The present experiment makes use of a 5.5-mm-diameter beam, for which the predicted efficiency drops to ~20%. We have also previously published an experimental study of the gain between two magnicon deflection cavities [6]. In this paper, we report the first operation of an entire magnicon circuit, leading

to the generation of high output power at 11.120 GHz, exactly twice the 5.560 GHz drive frequency.

II. APPARATUS

Figure 1 shows the experimental setup for the NRL magnicon experiment. The electron beam is produced on the NRL Long-Pulse Accelerator Facility [7] using a cold cathode positioned in the fringing fields of the main solenoidal magnet. The accelerator is a Marx generator that operates single shot, with an output voltage waveform that typically consists of a ~ 150 nsec risetime, a ~ 250 nsec voltage flat-top, and a ~ 800 nsec falltime that is related to diode impedance collapse. During the voltage falltime, the impedance collapse often results in substantially larger currents than during the voltage flat-top. This portion of the voltage waveform is often eliminated by use of a triggered divertor switch in the Marx generator, which shorts the Marx generator to ground through a 10Ω resistor. In recent operation, the beam parameters were increased beyond the design parameters to 650 kV and 225 A during the voltage flat-top in order to overcome a gain saturation effect, as described below.

The complete five-cavity circuit includes four deflection cavities (a drive cavity, two gain cavities, and a two-section π -mode penultimate cavity), all operating at 5.560 GHz in the TM_{110} mode, followed by an 11.120 GHz TM_{210} -mode output cavity with a Q of ~ 250 . The rf circuit is immersed in a uniform magnetic field of 6–11 kG. The cavities are fabricated from stainless steel, to allow for the penetration of pulsed magnetic fields, with a thin coating of copper that serves to decrease the ohmic losses. The cavities are held together with bolts, and make use of a combination of Viton O-rings to maintain the vacuum seals and copper gaskets to maintain the rf seals. The first cavity is driven by rf from a tunable C-band magnetron. Typical drive powers are 1–10 kW, but much lower values can be used to measure the linear gain of the deflection cavities.

Each of the deflection cavities has a calibrated rf pin (the first cavity) or loop to monitor the intracavity rf signal. The power from the TM_{210} output cavity is coupled through an iris into a 3.5-cm-diam. output waveguide ending in a lucite window. In order to produce single-mode output, the diameter of the output waveguide was made smaller than that of the output cavity. The magnicon output mode is TE_{21} , since the iris couples TE and TM modes with the same azimuthal symmetry, and the TM_{21} mode is cut off in the output waveguide. The beam current is monitored by means of a resistive current shunt built into the wall of the output waveguide. Rf output is measured using small waveguide pickups in the far field of the output window. The various rf signals are measured using calibrated attenuators and crystal detectors. All cavity properties and cold test frequencies are determined using a Hewlett-Packard HP 8350B sweep oscillator with an HP 83590A 2–20 GHz rf plug-in, and an HP 8757A scalar network analyzer, while power calibrations are carried out using an HP 432B power meter. Since the sweeper is also used as the local oscillator for heterodyne measurements, it serves as the overall frequency standard for the experiment.

In the design for this device [4], the externally driven fields in the first cavity induce a very small initial transverse momentum ($\alpha \sim 0.005$). This leads to rf amplification by approximately 13 dB in cavity 2 (the first gain cavity). The higher level of rf in this cavity then further increases the transverse momentum to $\alpha \sim 0.02$. This process, involving rf gain and increasing transverse momentum, proceeds through cavities 3 and 4, the remaining deflection cavities. Cavity 4, also known as the penultimate cavity, is a two-section cavity containing a π -mode. The use of the π -mode allows the electron to remain in a favorable phase for transverse momentum increase for twice the length permitted in a simple TM_{110} cavity. Since the penultimate cavity should contain rf fields that are a factor of ~ 5 larger than those of the preceding cavity, and since these fields interact with the electron beam for twice the length of the other deflection cavities, most of the transverse momentum should be developed here. In fact, sufficiently high fields in this cavity can be considered to be a prerequisite for generating high power radiation in the output cavity.

III. PRELIMINARY EXPERIMENTS

Initial tests of the magnicon circuit were carried out at the design voltage and current (500 kV, ~170 A), and at magnetic fields ranging from 6.5–10 kG. The deflection cavity gain is an increasing function of beam current and also of B/γ , where γ is the relativistic factor associated with the beam kinetic energy [8]. As a result, deflection cavity oscillation often occurred during the falling portion of the voltage pulse, due both to the higher current and the lower voltage. For that reason, the following discussion refers to signals observed during the voltage flat-top.

In the design calculations, a total of approximately 40 dB of rf gain occurs between the drive cavity and the penultimate cavity. In the actual experiment, operating at the design parameters, a small signal gain of ~40 dB was in fact observed at very low levels of drive power (<1 W). However, as the drive power was increased, on a shot-to-shot basis, the signal in each of the deflection cavities was seen to saturate in the range of 1–10 kW. For drive powers greater than 10 kW, there was no net gain in the deflection cavities. This very low power saturation of the deflection cavity rf signals is associated with the generation of plasmas in the deflection cavities. The presence of a plasma has been confirmed by observation of light emission from the cavities when the saturation effect occurs. Under these conditions, only small signals (<100 kW) were seen from the output cavity.

Studies were carried out of the rf saturation process using only the drive cavity. It was found that drive powers as high as 50 kW did not lead to this plasma effect unless either 1) an axial magnetic field of greater than 50–100 G was present, or 2) the accelerator was discharged into the electron beam diode. In either case, the threshold drive power to produce a plasma in the drive cavity dropped to ~1–10 kW. In the case of the magnetic field, there was a threshold effect, and stronger magnetic fields did not lower the power threshold. In the case of the electron beam diode, accelerator discharges with the cavity completely separated from the diode still initiated plasma loading of the drive cavity at low power, demonstrating that x-

radiation was involved. Apparently, the combination of x-rays, to provide a population of free electrons and to cause gas desorption from the cavity surfaces, and an axial magnetic field (parallel to the rf electric field of the TM_{110} mode) leads to a very low threshold for this plasma phenomenon. This effect is attributed to the inadequate vacuum and surface conditions typical of a pulsed power vacuum ($\sim 10^{-5}$ T), and to the inability to carry out high-temperature bakeout and rf conditioning, such as are employed in high power klystrons [9]. It seems appropriate to refer to this phenomenon as "plasma loading," since the cavity rf fields do not in fact vanish, but appear to establish an equilibrium level, based on the combination of external drive power and the plasma loading self-consistent with this drive power. This plasma constitutes a nonlinear load on the rf properties of the cavity, clamping the level of the microwave signal without completely shorting out the cavity. This phenomenon is distinct from true rf breakdown of the cavities, which can occur at very high levels of rf fields.

IV. HIGH POWER EXPERIMENTS

A major effort was made to improve the vacuum conditions. One of the limitations on the achievable vacuum pressure was the very limited vacuum conductance involved in pumping the deflection cavities through the beam pipe. This was improved by pumping the first three deflection cavities from the side through a pair of parallel pumping tubes that connect to the main diode vacuum. In addition, the cavities were disassembled, thoroughly cleaned with detergents and solvents, and then reassembled and put through a low-temperature ($\sim 120^\circ$ C) bakeout. Following this, a new set of measurements was begun.

In initial measurements, the low power saturation effect was still seen during the voltage flat-top under the usual conditions of current and voltage. In order to overcome the plasma loading effect, the experimental parameters were varied in order to greatly increase the rf gain of the deflection cavities. First, the voltage was increased from 500 kV to 650 kV, resulting in a higher beam current. Second, the axial magnetic field (or rather B/γ) was

increased. Higher magnetic fields further increase the beam current. In addition, as discussed previously, deflection cavity gain increases both with current and with B/γ .

Initial measurements were carried out at 650 kV, 300 A, and 11 kG. Under these conditions, the rf gain process can overcome the low power saturation caused by plasma loading. Figure 2 shows traces of magnetron monitor, the beam voltage and current, the cavity 1 signal, a heterodyne signal resulting from mixing the cavity 1 signal with a local oscillator tuned to the magnetron frequency, and signals from cavities 2, 3, 4 and 5 (the output cavity, which is monitored at the output window). (The heterodyne signal is used to tune the magnetron frequency to a frequency set on the HP 8350B sweeper, which is used as the local oscillator, and also to observe the effect of the beam on the phase of the rf in cavity 1.) The result is a short (~50 nsec FWHM) rf gain spike in the penultimate cavity, followed in temporal sequence by gain spikes in the third and second deflection cavities (see Fig. 2). This temporal sequence is due to the fact that the penultimate cavity has the highest total gain with respect to the drive signal, while the second deflection cavity has the least. Each of the cavity signals in the second, third, and penultimate cavities ramp up to high levels (~80–90 dBm), and then suffer a complete rf breakdown. At the time of the rf maximum in the penultimate cavity, a small rf signal was observed at the output of the experiment (<100 kW).

These experiments demonstrated that sufficiently high gain could “burn through” the plasma saturation effect. However, at this very high magnetic field, the deflection cavities are not stable, and will ramp up to high power without a drive signal in the first deflection cavity.

A. Heterodyne Measurements

In order to diagnose the output, a new heterodyne diagnostic was constructed to measure the spectrum of the output radiation. This diagnostic combines the output signal with the signal from a tunable local oscillator in a double-balanced mixer, and then acquires the resulting signal using a Tektronix DSA602 digital oscilloscope with an analog bandwidth of ~1 GHz, a 2 GS/s digitizing rate, and an FFT (fast Fourier transform) capability. Figure 3

shows a block diagram of the heterodyne diagnostic. This diagnostic yields a measurement of $|\Delta f| = |f - f_{LO}| < 1$ GHz to a precision of a few MHz, where f is an emission line from the experiment and f_{LO} is the selected frequency of the local oscillator. By varying the local oscillator frequency on a shot-to-shot basis to remove ambiguities in the sign of Δf , and to rule out signals due to aliasing, spectral features can be determined to a precision of a few MHz in the frequency range of 2 to 20 GHz. (The absolute frequency standard is the same HP 8350B sweeper used for cavity cold tests, and which is here used as the local oscillator.)

Using this diagnostic, a search was made for the predicted magnicon output frequency of 11.120 GHz. At the higher magnetic fields (~11 kG) that maximized the deflection cavity gain (see Fig. 2), only low frequency components (<9.5 GHz) were observed in the output rf pulse. However, as the magnetic field was reduced, the predicted magnicon line appeared in the emission spectrum. At magnetic fields ranging from 6.7–8.2 kG, the dominant spectral feature, and the only spectral peak at frequencies greater than 9.5 GHz, was a strong feature at 11.120 GHz. A typical signal trace from the mixing crystal, and its FFT, are shown in Fig. 4, displaying the 11.120 GHz feature. For this shot, the local oscillator was set to 10.700 GHz, and the FFT measured a frequency shift of 420 MHz. The spectral feature at 11.120 GHz was present on every shot, responded appropriately to variations of the local oscillator frequency, and also vanished if the microwave signal (before mixing) was filtered using $f < 8$ GHz or $f > 12$ GHz filters. These tests demonstrated that the frequency was correctly identified.

Figure 5 shows a complete set of experimental traces corresponding to conditions under which high power emission at 11.120 GHz was observed. The magnetic field for this shot was 7.9 kG. The magnetron was tuned to 5.560 GHz, and was discharged into the first cavity in advance of the voltage pulse. On this shot, the diode voltage waveform was terminated after the voltage flat-top using the divertor switch in the Marx generator, in order to avoid the cavity oscillations that often occur during the falling portion of the voltage waveform. The first cavity signal corresponds to ~400 W, the second cavity signal to ~500

W, and the third cavity signal to ~ 2 kW. On this shot, cavities 2 and 3 are demonstrating the gain saturation mechanism described previously. Nevertheless, the penultimate cavity signal reaches ~ 680 kW in a narrow gain spike, before breaking down. The result is a large signal from cavity 5 (the output cavity), where the pickup is in the far field of the output window. Under these conditions, most of the gain is occurring between the third and fourth cavities, and the fourth cavity is clearly operating very close to instability.

B. Far-field Measurements

In order to characterize the output cavity emission, a far-field measurement setup was constructed (see Fig. 6). In order to ensure that only the 11.120 GHz frequency component would be measured during mode scans, K_u -band waveguide-to-coax adapters, with a 9.5 GHz cutoff frequency, were used as the microwave pickups. Two pickups, one stationary, and one that swept in the horizontal plane on an 81.3-cm-radius arc about the center of the 3.5-cm output window, were used to measure the radiation antenna pattern. An anechoic enclosure was built around the pickups and the output window. Typical experimental traces for the penultimate cavity and the two far-field pickups are shown in Fig. 7, along with the voltage waveform. The results for the E_θ and E_r scans are shown in Fig. 8. Each plotted point in Fig. 8 is the average of three experimental shots, and the value from each shot is normalized by the power measured at the stationary pickup. (The data only extends from -75° to $+40^\circ$, because the stationary pickup was positioned at $+50^\circ$.) Fig. 8 also shows the calculated far-field radiation pattern for the TE_{21} mode, with the height of the E_θ curve normalized to the peak of the experimental data. The calculation is carried out assuming the presence of a rotating, or circularly-polarized mode, since the scanning-beam interaction in the output cavity should couple to a single circular polarization. The data is clearly in good agreement with the calculated mode pattern. None of the other four available non-cutoff modes in the output waveguide at 11.12 GHz have far-field patterns that resemble the experimental data. This, combined with the frequency measurements, confirms the

identification of the magnicon mode. However, the lack of a stronger dip in the near-axis signal suggests the presence of some conversion into the TE_{11} mode in the output waveguide, or alternatively, some reflections in the experimental setup for the far-field measurements.

Using the experimental data in Fig. 8, one can relate the power received by a K_u -band pickup at the angular peak of the pattern to the total power radiated from the output window into 2π . (It is assumed that the scanned horizontal radius is typical.) The method of calculating the power on each shot is illustrated in Table I. With the rf pickup oriented to receive the E_θ component of the far field pattern, the power (in dBm) measured at a calibrated crystal detector is increased by the measured attenuation through all the coaxial components up to the rf pickup ($+39.7 \pm 0.5$ dB). (This attenuation factor was measured in a single step to minimize errors.) Next, it is increased by the ratio, expressed in dB, of the solid angle of the rf pickup to 2π ($+45.2 \pm 0.5$ dB). In order to correspond to the actual antenna pattern, this must be decreased by the ratio between the average and peak of the antenna pattern (-3.7 ± 3 dB). This value was determined by using the experimental measurements between 0 and -75° . Based on the measurements, the result is increased by ($+2.5 \pm 0.25$ dB) to correct for the additional power radiated into E_r . Finally, there are two small corrections. First, the loss in the K_u -band waveguide-to-coax adapter, which is being used out of its normal frequency band, was measured at 11.120 GHz ($+1.0 \pm 0.2$ dB). Second, there is a small theoretical correction ($+0.7 \pm 0.2$ dB), based on the ratio between the effective and physical apertures of a rectangular pickup [10,11].

The best measured power varied somewhat from day to day (as is typical of many pulsed power experiments). The largest measured signals at the peak of the antenna pattern were in the range of 16.0 ± 0.5 dBm. Summing all of the loss factors, this corresponds to a total radiated power of ~ 101.4 dBm, or 14 MW, as shown in Table I, corresponding to an efficiency of $\sim 10\%$. While each of the correction factors contributes to the overall error bar, the uncertainty in the total power depends principally on the determination of the ratio between the signal at the angular peak and the total power radiated into 2π . This is subject both to

shot-to-shot variation and to the overall uncertainty in determining the average value of the ratio. The shot-to-shot variation in the ratio can be estimated by examining the shot-to-shot variation in the ratio between the power measurements at two stationary pickups. Typically, the two pickups agree to within ± 1 dB. The overall uncertainty in determining the average could be reduced by making measurements out of the horizontal plane. However, the measured radius should be typical of the entire antenna pattern, because the circularly-polarized mode of the output cavity should radiate equally into all azimuthal angles. The close agreement between the calculated and measured patterns in both E_r and E_θ , which sample fields from two orthogonal linearly polarized components of the antenna pattern, support this interpretation. The overall error bar is estimated to be ± 3 dB.

Next, a scan of output power versus magnetic field was made with one pickup at the angular maximum of the antenna pattern. The results are shown in Fig. 9. The power is seen to peak experimentally at ~ 8 MW in the vicinity of 7.3 kG, and to vanish both below 6.5 kG and above 8.5 kG. [The 14 MW signals discussed previously were not found during this particular scan.] The reason for the loss of high power emission at lower magnetic fields is easily understood. It is observed that high power emission only occurs when there is a large rf signal in the penultimate cavity. This large rf signal becomes erratic below 7 kG, and vanishes completely (during the voltage flat-top) below 6.5 kG. The transverse momentum needed to drive the magnicon mode is not available at lower magnetic fields, because the lower gain puts the experiment back into the regime for which plasma loading clamps the penultimate cavity rf fields at a low level.

C. Simulations

The loss of the magnicon signal at higher magnetic fields calls for a different explanation. It is observed that the large penultimate cavity signal persists at all higher values of magnetic field (through 11 kG), and should provide the required transverse beam momentum to drive the output cavity interaction. In order to examine the predicted behavior

of the output cavity as a function of magnetic field, a set of time-dependent simulations of the output cavity were carried out, assuming a constant value of $\alpha=0.5$, and $\theta_{sc0}=90^\circ$, where θ_{sc0} is the scanning angle spread [12]. (Scanning angle spread is defined as the instantaneous angular extent of the guiding centers of the electrons in the beam, as viewed from the axis of the cavity.) This value of α was chosen to yield approximately the same peak power as the experimental value, with the scanning angle spread corresponding to the initial beam diameter. These output cavity simulation results are shown in Fig. 9. It is noteworthy that these output cavity simulations predict high power output over a much broader range of magnetic fields ($P>2$ MW for $6.5<B_z<11$ kG) than is observed in the experiment.

In order to understand the parametric dependence of the output power on magnetic field, and the discrepancy between experiment and output cavity simulations, the INP magnicon code (see [4] and references therein) was used to determine the effect of operating the experiment in a situation in which most of the beam spin-up occurs in the penultimate cavity. The magnicon code uses a steady-state model that makes use of the phase synchronism between the beam and the rotating rf waves. This phase synchronism means that electrons entering the system at different times describe trajectories that are identical except for their spatial phase, and that the phase of the trajectories and the phase of the rf advance together at the rf drive frequency. Thus, the entire simulation can be carried out by following a single temporal slice of electrons that is one macroparticle deep in z . A finite diameter electron beam is broken up into a number of macroparticles, typically 37, spread uniformly over the beam cross section. The beam is modeled with zero initial pitch angle, to model a magnetic-field-immersed diode. Solutions for the realistic rf fields of each cavity are an input to the particle simulation code, which then assumes a particular amplitude and phase of these fields in each of the cavities, and integrates the full Lorentz equations for the electrons through these fields using the third-order Runge-Kutta method. During the integration, energy losses and cavity detunings are also calculated. The amplitudes and phases of the fields in each cavity are input parameters, and are typically adjusted by iteration until power balance is

obtained in all of the cavities at the correct rf phase. The correct rf phase in a particular cavity is assumed to be the phase that extracts the maximum energy from the electrons.

The magnicon code predicts that the penultimate cavity will be unstable over a broad range of magnetic fields, and can reach high power without being driven by the first cavity. That is, energy balance can be obtained in the penultimate cavity at high levels of rf field using a beam with no initial transverse momentum that experiences no rf fields in the first three deflection cavities. This simulation result is not in complete agreement with the experimental data, which indicate that, over the magnetic field range for which 11.120 GHz emission is observed from the output cavity, a signal from the driver magnetron is generally required in the first cavity in order to induce large rf fields in the penultimate cavity during the voltage flat-top. The penultimate cavity traces from the experiment indicate that the fields build up rapidly when the first cavity is driven, and then suffer an rf breakdown. Based on a calibration of the fourth cavity pickup, the maximum observed fields in the fourth cavity correspond to rf powers of 500 kW to 1 MW, based on the measured cold cavity Q of ~ 8000 . This indicates that the maximum H -fields in the cavity are in the range of 50 to 60 kA/m.

The magnicon code predicts that fields this large can result from self-excitation (instability) of the penultimate cavity at magnetic fields above 7.2 kG. Below this magnetic field, the code indicates that some prior beam excitation from cavities 1-3 is needed to drive the penultimate cavity to this level of rf fields.

Accordingly, for the code runs above 7.2 kG, the fields in the first three cavities were assumed to be zero, while the fields in the fourth cavity were varied at levels below the point at which the code predicts that they would saturate. The amplitude and phase of the rf fields in the output cavity were then varied to find the correct phase, and the field level that gave power balance based on the output cavity Q of ~ 250 . For the case of 6.95 kG, for which the simulation code does not predict self-excitation, fields were assumed in the third cavity sufficient to drive the fourth cavity to power balance at a particular field level, and iteration was again used to find the self-consistent operating point of the output cavity. For this

purpose, the third cavity fields were varied within a range consistent with the power observed from the third cavity (<10 kW power) in the experimental measurements. (Assuming similar third cavity fields for the higher magnetic field cases did not have much effect on the predicted output power.)

Figure 9 plots the results from the magnicon code simulations. At each magnetic field, the output power is optimized as a function of penultimate cavity field. (Since these are steady-state simulations, this procedure amounts to finding the best value of the penultimate cavity fields that occurs during the power ramp that eventually leads to rf breakdown of the penultimate cavity.) These simulations are in good agreement with the experimental results, and predict the rapid fall-off in output power as the magnetic field is increased above 7.5 kG. The highest power simulation point at 6.95 kG, which is somewhat above the highest powers measured in this particular scan, in fact agrees well with the best measured powers that were discussed previously. Experimental operation was observed to become increasingly erratic below 7.2 kG, as the lower gain frequently reduced the magnitude of the penultimate cavity signal. The lack of high power operation below 6.5 kG is also consistent with the simulations, since this corresponds to conditions under which the self-consistent penultimate cavity rf fields are too low to drive high power emission in the absence of large fields in the gain cavities. We know from the experiment that under these conditions, the penultimate cavity saturates at low power due to plasma loading. When this happens, there is no high power emission at 11.120 GHz.

Figure 10 shows a summary of results from the simulation code. Output power is plotted versus the penultimate cavity rf field at several different applied magnetic fields. At each magnetic field, the mean beam α corresponding to the optimum value of rf magnetic field is also indicated. It is noteworthy that the output power, optimized as a function of the penultimate cavity rf field, is a strong function of the axial magnetic field. Over the range studied, the output power increases monotonically as the axial magnetic field is reduced. At the same time, the fourth cavity rf fields that optimize the output power steadily decrease as the

magnetic field is increased. For a given magnetic field, there is an optimum value for the penultimate cavity rf field, and further increasing the rf field above that value results in lower predicted output powers. Figure 10 also shows the mean beam α at the entrance to the output cavity for the optimum point at each magnetic field. The code demonstrates that the optimum α progressively decreases as the magnetic field is increased. The reason for this behavior is not well understood.

Figure 11 shows a typical simulation of the experiment. The axial magnetic field is assumed to be 7.2 kG. The penultimate cavity rf field is assumed to be 55 kA/m. The predicted output power is 8.05 MW at 5.5% efficiency. The average pitch angle produced by the penultimate cavity is $\sim 28^\circ$, corresponding to $\alpha \sim 0.54$. For the same penultimate cavity fields, an optimized single particle simulation at the same magnetic field gives an efficiency of 21.5%. It is evident from this that the efficiency of the output cavity is dominated by the large spreads in energy and momentum produced by the penultimate cavity fields. Apparently, the effect of these spreads becomes increasingly deleterious as the magnetic field increases, yielding the results shown in Fig. 10. Based on a Q of 8000 for the penultimate cavity, a field of 55 kA/m corresponds to an intracavity power of ~ 1.1 MW. Based on the calibration of the sidewall pickup of the penultimate cavity and all the related microwave components, the largest signals observed in the penultimate cavity correspond to ~ 900 kW, in reasonable agreement with this value.

One of the experimental observations, visible in Fig. 5, is that the temporal peak of the output cavity signal often occurs ~ 20 – 50 nsec earlier than the peak of the penultimate cavity signal. However, while wall damage around the apertures of the penultimate cavity provides clear evidence of the rf breakdown that terminates the penultimate cavity signal, resulting in the transient gain spike seen in Fig. 5, there is no sign of breakdown damage on the walls of the output cavity. There is also no evidence of breakdown at the vacuum window at the end of the experiment. However, the simulation results summarized in Fig. 10 suggest a possible explanation for the phenomenon. For a given magnetic field, there is an optimum field in the

penultimate cavity that maximizes the output cavity power. Higher than optimum penultimate cavity fields decrease the power because of the effects of the energy and momentum spreads induced on the electron beam. As an example, the transient operation of the experiment at 7.4 kG would correspond to moving to the right along the set of points in Fig. 10 corresponding to 7.4 kG. In this example, the output power would rise until a penultimate cavity field of 45000 A/m is reached, and then decrease down to zero as the field continues to increase. This suggests that the decrease in output power while the penultimate cavity fields are still rising may result from overdriving the electron beam.

V. SUMMARY AND CONCLUSIONS

The NRL magnicon experiment previously demonstrated the basic magnicon gain mechanism in two-deflection-cavity experiments. However, those experiments were forced to operate at very modest power levels to avoid an unanticipated gain saturation effect, that occurred as intracavity powers approached the kilowatt level. In the test of the full five-cavity magnicon circuit, the same gain saturation effects were observed despite substantial improvements in the overall vacuum system. Experimental tests demonstrated that the saturation was due to plasma loading, caused by inadequate vacuum and surface conditions, and initiated by the large x-ray flux from the accelerator diode region. A program of progressively improving the vacuum conditions, while at the same time pushing the envelope of magnicon parameters by operating at higher current, voltage, and magnetic field, has demonstrated that this low power saturation effect can be overcome. The result is to produce short (~50–200 nsec) high power pulses in the deflection cavities, generally followed by rapid rf breakdown. Under the right combination of experimental parameters (650 kV, 225 A, 6.7–8.2 kG magnetic field), a large amplified signal is observed in the penultimate cavity at 5.560 GHz. The amplitude and duration of this signal are limited by rf breakdown. Synchronous with the penultimate cavity signal, a ~100 nsec FWHM frequency-doubled output pulse is observed at 11.120 GHz. The signal is precisely twice the measured 5.560

GHz frequency of the penultimate cavity signal, indicating excitation of the synchronous magnicon mode. A scan of the far-field antenna pattern confirms that the output power is in the predicted TE_{21} mode (with the output cavity operating in the TM_{210} mode). Based on absolute calibration of the detected microwave signals, the best shots correspond to $14 \text{ MW} \pm 3 \text{ dB}$ at an efficiency of $\sim 10\%$.

The experimental results demonstrate that the output cavity is driven by the penultimate cavity. The presence of a large penultimate cavity signal during the voltage flat-top is a prerequisite for high power operation of the output cavity. In addition, the shot-to-shot variation in the timing of the penultimate cavity signal is tracked by the timing of the output cavity signal. Furthermore, the magnicon appears to be operating as an amplifier, since, at the optimum magnetic fields ($\sim 7.2 \text{ kG}$), the penultimate cavity signal is only present (during the voltage maximum) if the 5.560 GHz drive signal is present in the first deflection cavity. However, the present operating regime is clearly very close to instability (and is unstable in the simulations), with most of the gain occurring in the penultimate cavity as part of a rapid ramp to high power that is typically terminated by rf breakdown of the penultimate cavity. We have not yet determined the required drive power to produce the output cavity signal, the bandwidth of the interaction, or the degree to which the output signal is frequency or phase locked to the drive signal. We have also not found a feasible means to eliminate the plasma effect in the present experiment, in order to operate in a regime of stable penultimate cavity gain.

Work is in progress to further characterize and optimize the operation of the present magnicon experiment. However, it seems evident that the NRL program must transition to a thermionic diode, a cw magnet, a rep-rated modulator, and an ultrahigh vacuum environment in order to demonstrate the feasibility of efficient, long-pulse, high-duty-factor magnicon amplifiers at 11.4 GHz for linear accelerator applications.

ACKNOWLEDGMENTS

We are grateful for the collaboration with O.A. Nezhevenko and V.P. Yakovlev in the design of the magnicon circuit, and for the assistance of C.A. Sullivan in earlier phases of the experiment. This work was supported by the U.S. Department of Energy under Interagency Agreement DE-AI02-94ER40861.A001, and by the Office of Naval Research.

REFERENCES

1. M. Karliner, E.V. Kozyrev, I.G. Makarov, O.A. Nezhevenko, G.N. Ostreiko, B.Z. Persov, and G.V. Serdobintsev, "The Magnicon—An Advanced Version of the Gyrocon," *Nucl. Instrum. Methods Phys. Res.*, vol. A269, pp. 459–473, 1988.
2. O.A. Nezhevenko, "Gyrocons and Magnicons: Microwave Generators with Circular Deflection of the Electron Beam," *IEEE Trans. Plasma Sci.*, vol. 22, pp. 756–772, October 1994.
3. W.M. Manheimer, "Theory and Conceptual Design of a High-Power Highly Efficient Magnicon at 10 and 20 GHz," *IEEE Trans. Plasma Sci.*, vol. 18, pp. 632–645, 1990.
4. O.A. Nezhevenko, V.P. Yakovlev, S.H. Gold, and B. Hafizi, "Design of a High Power X-Band Magnicon Amplifier," *IEEE Trans. Plasma Sci.*, vol. 22, pp. 785–795, October 1994.
5. B.A. Baryshev, I.V. Kazarezov, E.V. Kozyrev, G.I. Kuznetsov, I.G. Makarov, O.A. Nezhevenko, B.Z. Persov, M.A. Tiunov, V.P. Yakovlev, and I.A. Zapryagaev, "A 100 MW Electron Source with Extremely High Beam Area Compression," *Nucl. Instrum. Methods Phys. Res.*, vol. A340, pp. 241–258, 1994.
6. S.H. Gold, C.A. Sullivan, B. Hafizi, and W.M. Manheimer, "Study of Gain in C-Band Deflection Cavities for a Frequency-Doubling Magnicon Amplifier," *IEEE Trans. Plasma Sci.*, vol. 21, pp. 383–387, August 1993.
7. N.C. Jaitly, M. Coleman, S. Eckhouse, A. Ramrus, S.H. Gold, R.B. McCowan, and C.A. Sullivan, "1 MV Long Pulse Generator with Low Ripple and Low Droop," in *Digest of Technical Papers—Eighth IEEE International Pulsed Power Conf.*, IEEE Catalog No. 91CH3052–8, edited by K. Prestwich and R. White (IEEE, New York, 1991), pp. 161–165.
8. B. Hafizi, Y. Seo, S.H. Gold, W.M. Manheimer, and P. Sprangle, *IEEE Trans. Plasma Sci.*, vol. 20, pp. 232–239, 1992.

9. G. Caryotakis, "'High-Power Microwave' Tubes: In the Laboratory and On-Line," *IEEE Trans. Plasma Sci.*, vol. 22, pp. 683-691, October 1994.
10. C.A. Balanis, *Antenna Theory*. New York: Harper & Row, 1982, Chapter 11.
11. L.J. Chu, "Calculation of the Radiation Properties of Hollow Pipes and Horns," *J. Appl. Phys.*, vol. 11, pp. 603-610, Sept. 1940.
12. A.W. Fliflet and S.H. Gold, "Theory of Competition between Synchronous and Nonsynchronous Modes in a Magnicon Output Cavity," *Phys. Plasmas*, vol. 2, pp. 1760-1765, May 1995.

Table I. Total Radiated Power Calculation

16.0 ± 0.5 dBm	Peak detected signals (E_{θ})
+ 39.7 ± 0.5 dB	Calibrated coax attenuation factor
+ 45.2 ± 0.1 dB	Geometric area factor
- 3.7 ± 3 dB	Ratio of average to peak of antenna pattern
+ 2.5 ± 0.25 dB	Power in E_r Polarization
+ 1.0 ± 0.2 dB	Calibrated pickup loss
+ <u>0.7 ± 0.2 dB</u>	Effective aperture correction
101.4 ± 3 dBm	Total power (14 MW)

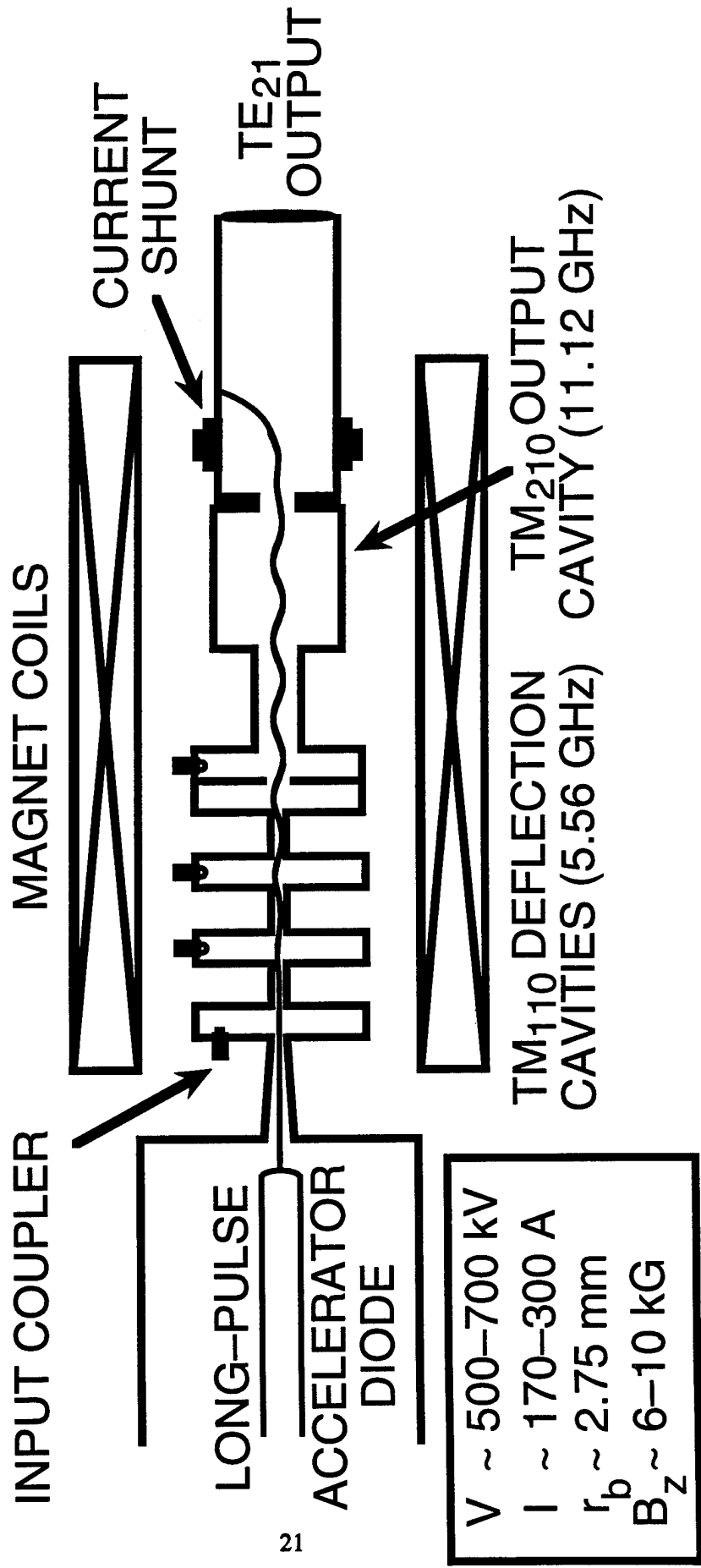
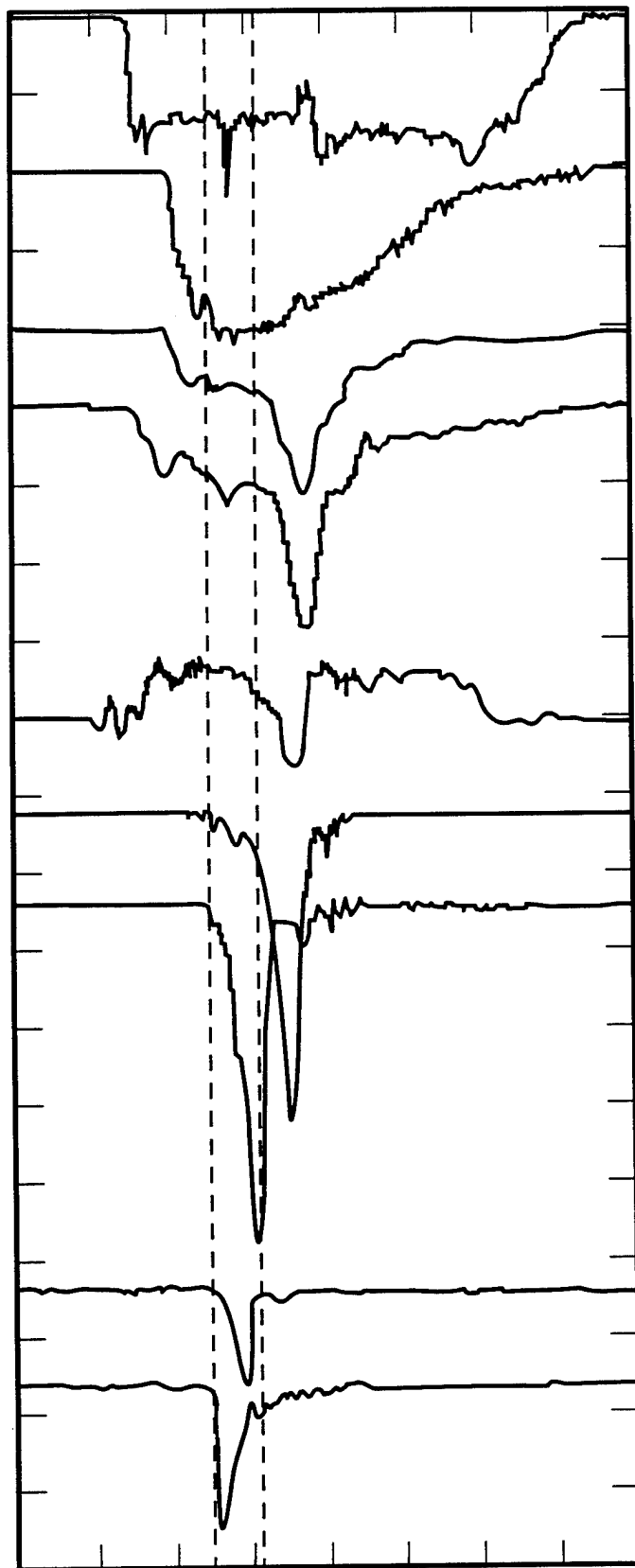


Fig. 1. Schematic diagram of the NRL X-band magnicon amplifier experiment.



MAGNETRON

V_D
(~ 650 kV)

I_{beam}
(~ 300A/900A)

CAVITY 1
(~ 60 dBm)

HETERODYNE
SIGNAL

CAVITY 2
(~ 73/88 dBm)

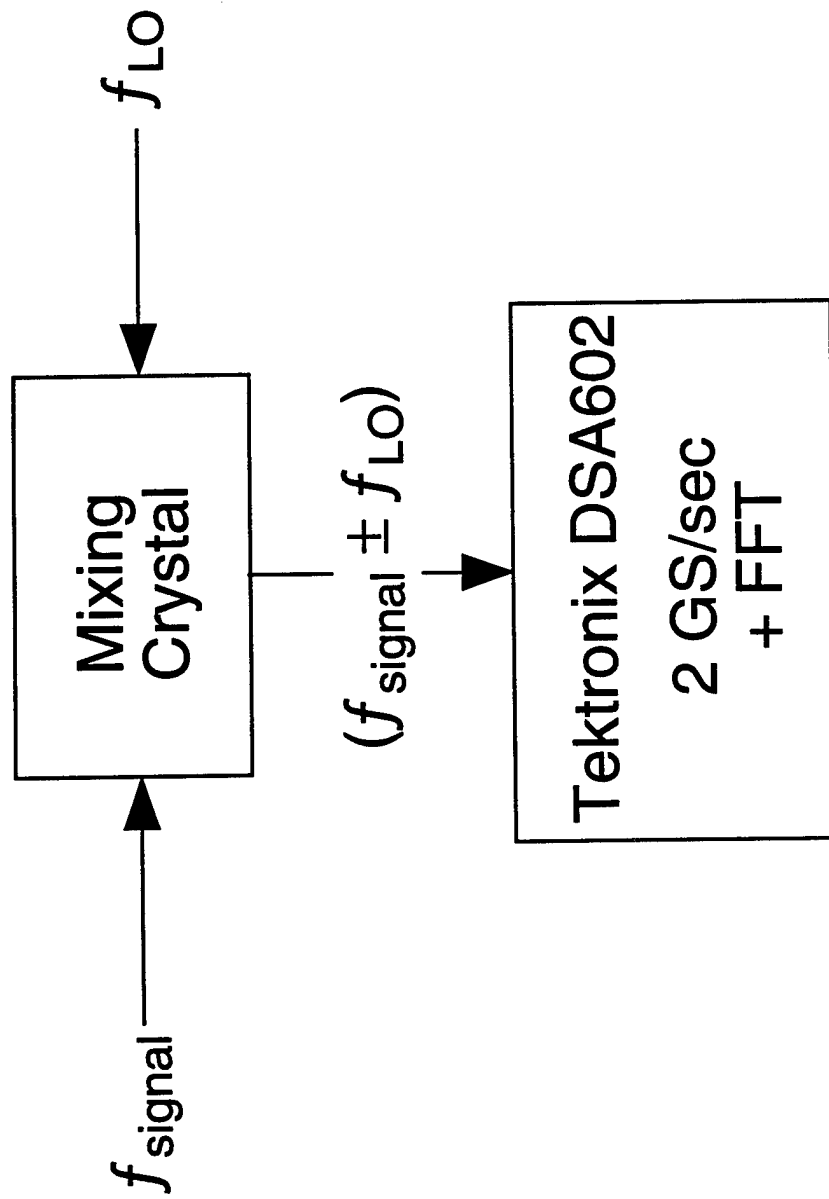
CAVITY 3
(~ 89 dBm)

CAVITY 4
(~ 79 dBm)

CAVITY 5
(~ 70 dBm)

200 ns/div

Fig. 2. Oscilloscope traces corresponding to operation at 650 kV, 11 kG.



$$\Delta f = |f_{\text{signal}} - f_{\text{LO}}| < 1 \text{ GHz}$$

Fig. 3. Block diagram of heterodyne frequency diagnostic.

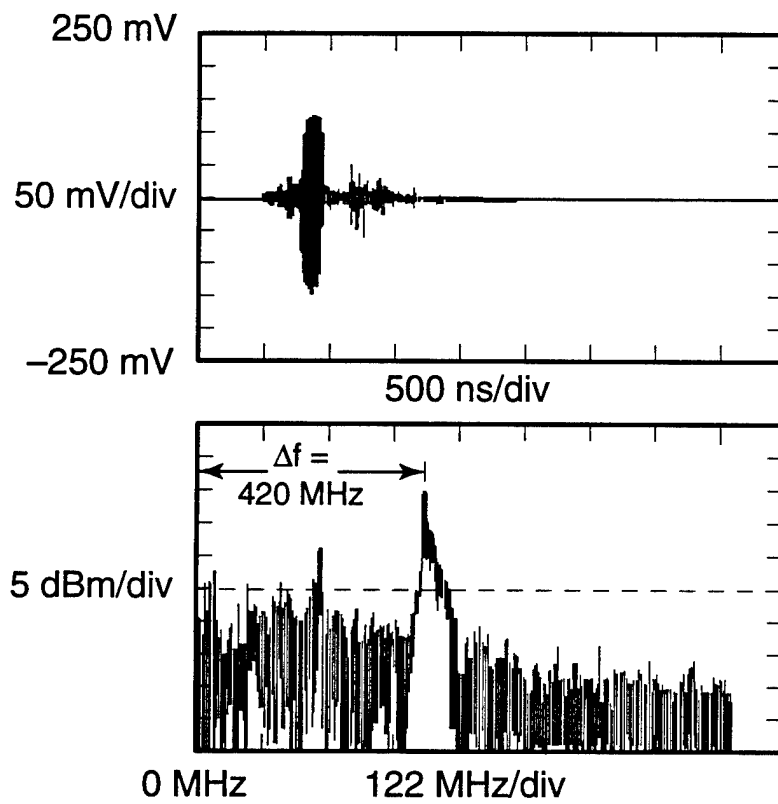


Fig. 4. Waveform from output microwave pulse mixed with local oscillator set to 10.700 GHz (top), and fast Fourier transform of waveform (bottom), showing the emission line at 11.120 GHz.

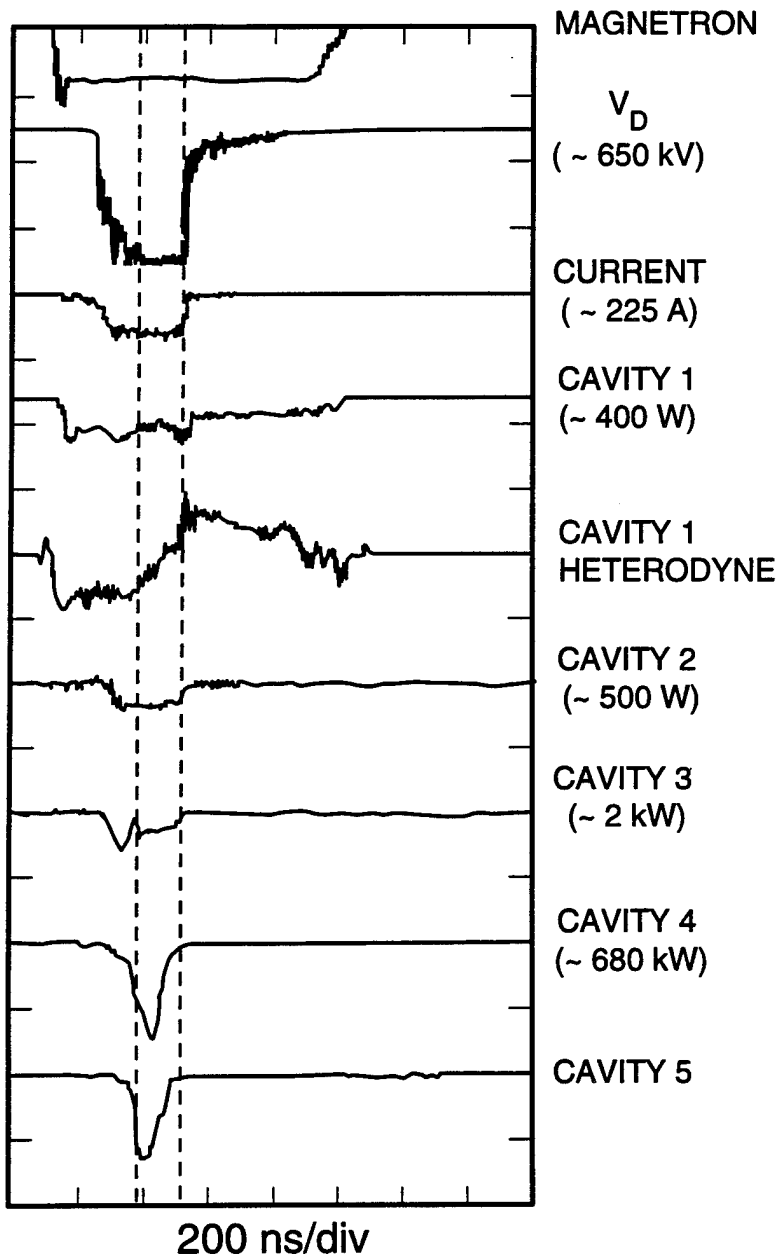


Fig. 5. Oscilloscope traces corresponding to magnicon operation at 650 kV, 7.9 kG.

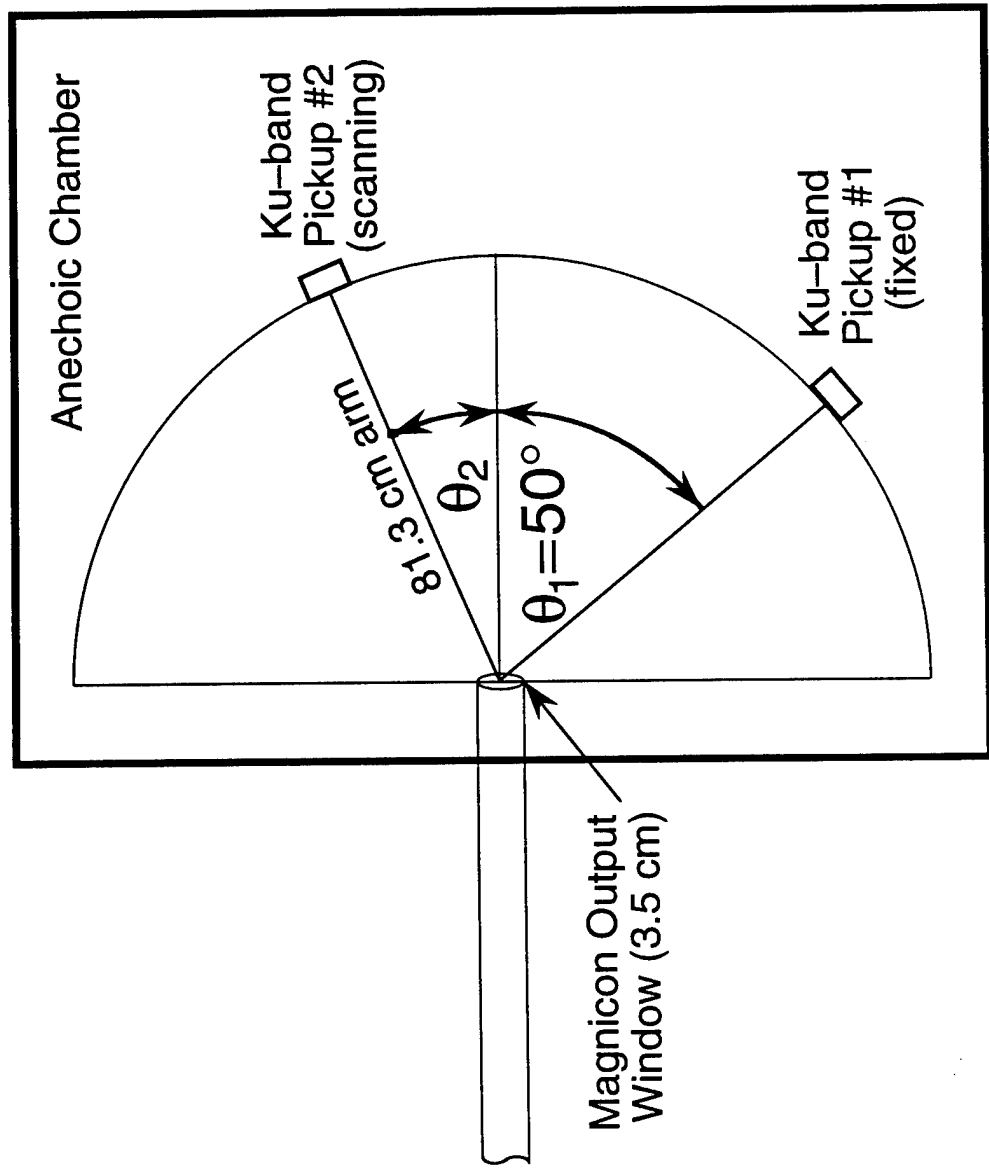


Fig. 6. Schematic diagram of far-field measurement setup.

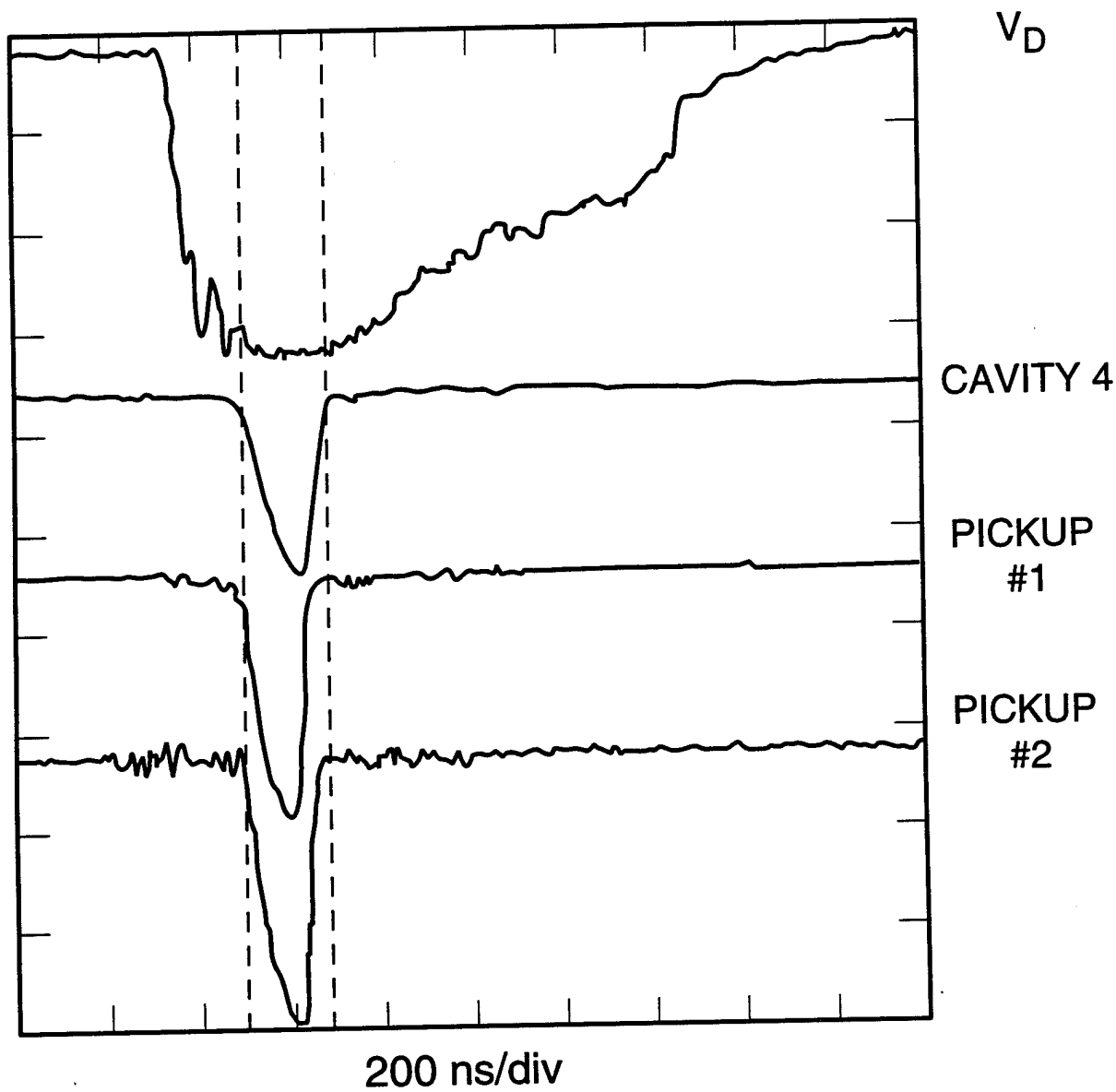


Fig. 7. Oscilloscope traces for measurement of far field antenna pattern of magnicon mode, showing voltage pulse, penultimate cavity microwave trace, and signal from two far-field microwave pickups.

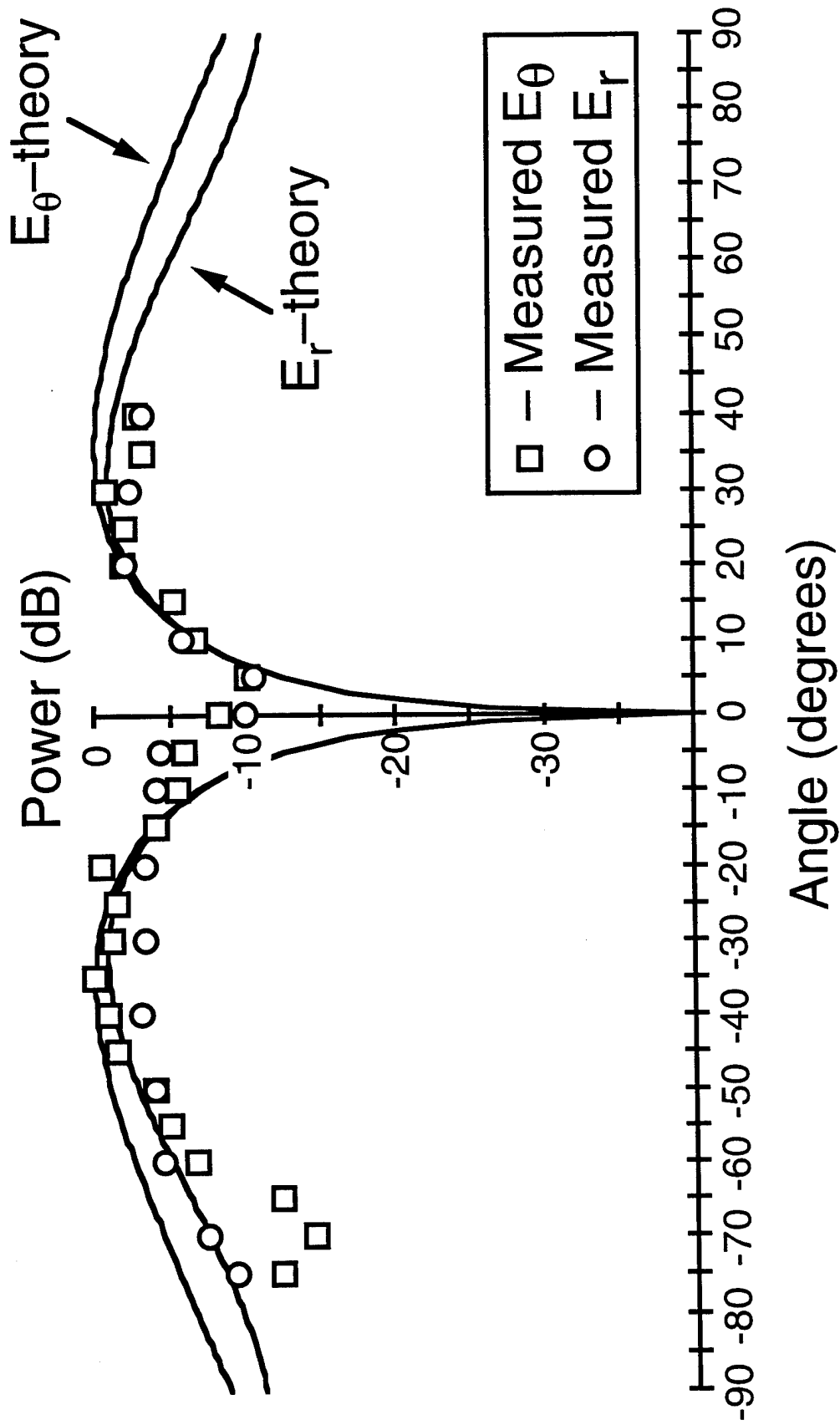


Fig. 8. Measured far-field antenna pattern from 3.5-cm-diam. output compared to predictions of theory for the TE₂₁ mode.

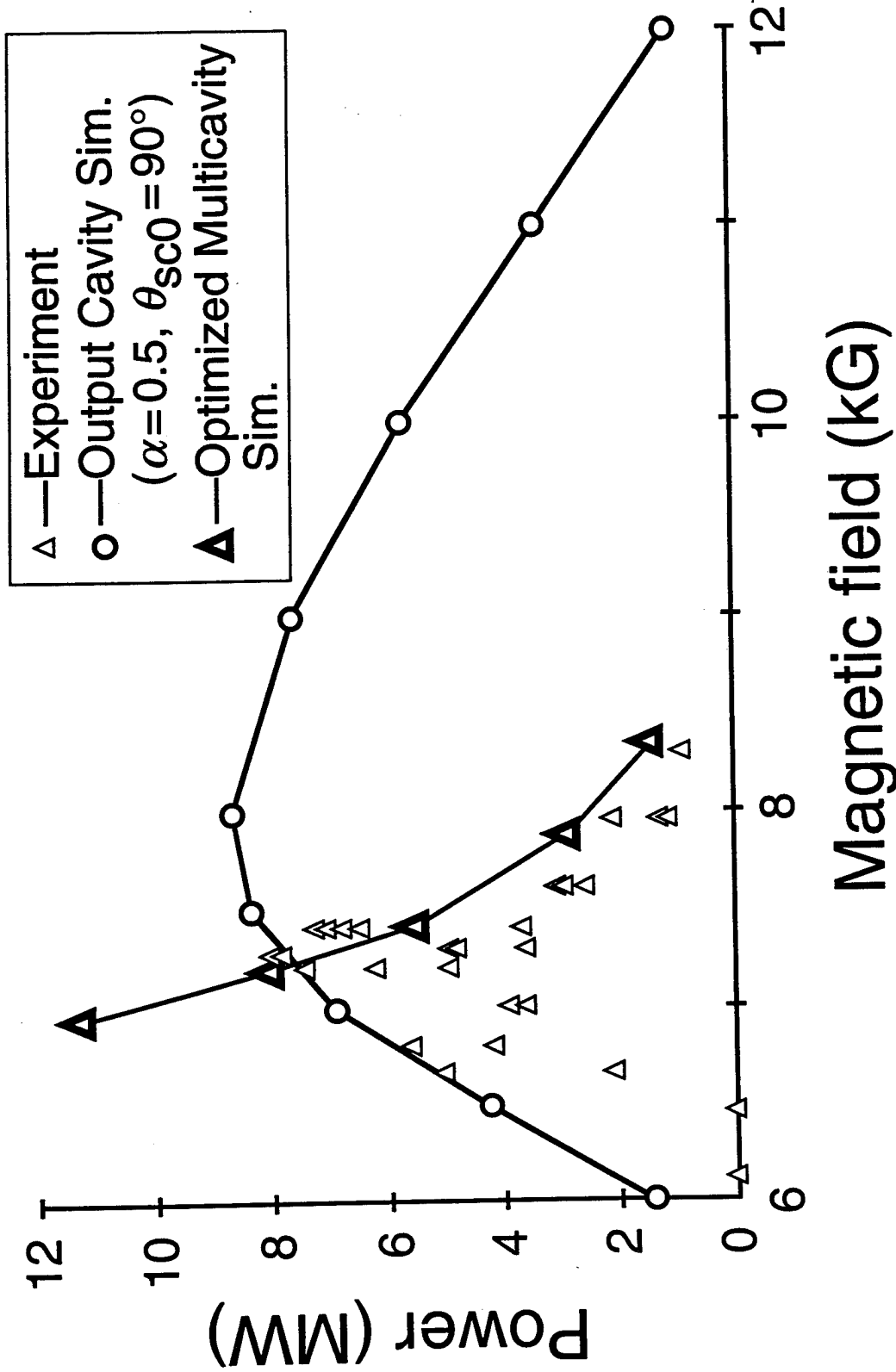
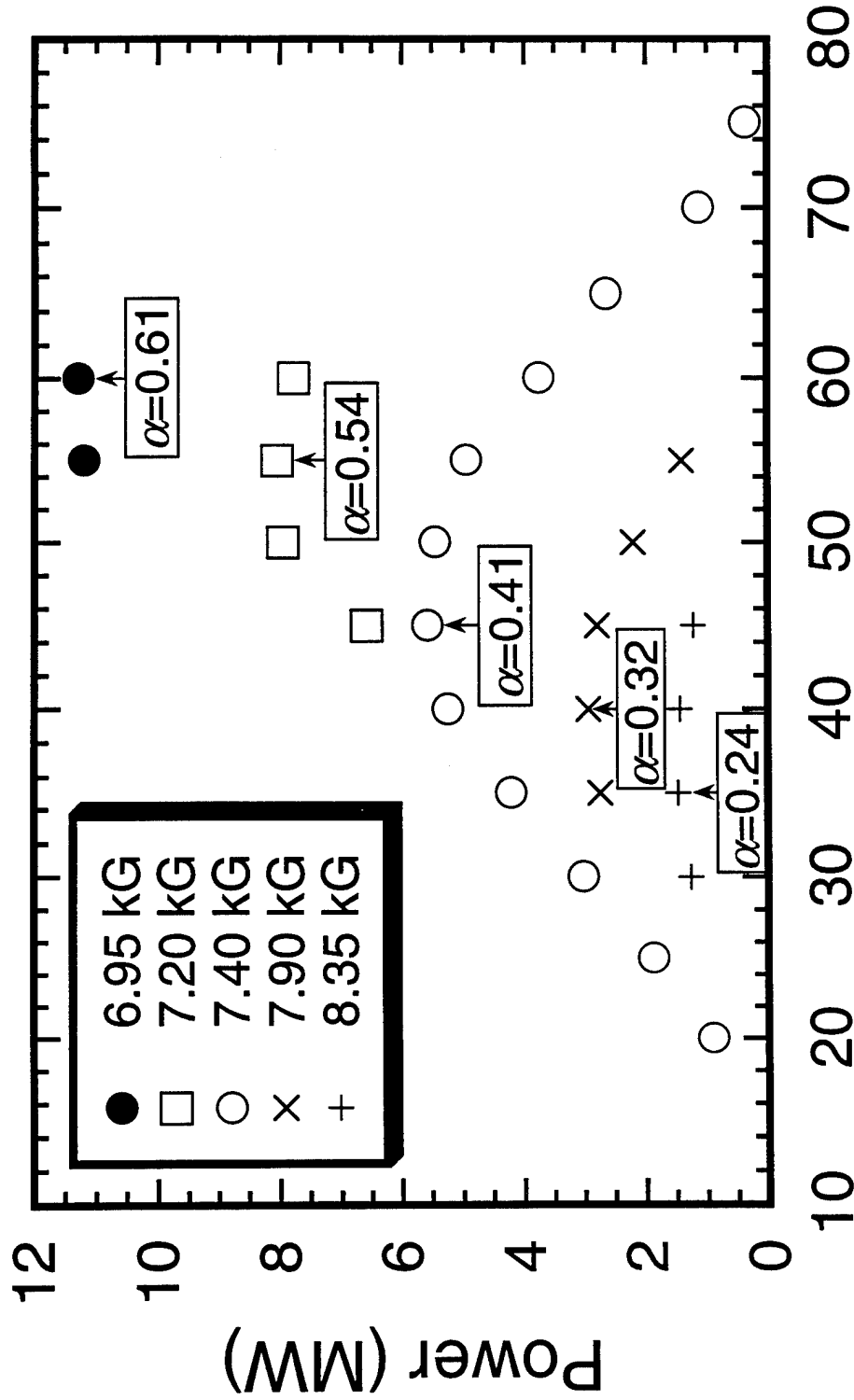


Fig. 9. Measured output power versus magnetic field, compared with predictions of theory. Small triangles are data from single experimental shots. Circles are results from a time-dependent output cavity simulation assuming $\alpha=0.5$ and $\theta_{sc0}=90^\circ$. Large triangles are the results from an optimized multicavity steady-state magnicon simulation.



Penultimate Cavity Field (kA/m)

Fig. 10. Predicted power versus penultimate cavity rf field from multicavity steady-state magnicon simulation. The beam α of the central electron at the entrance to the output cavity is shown for the optimum case at each magnetic field.

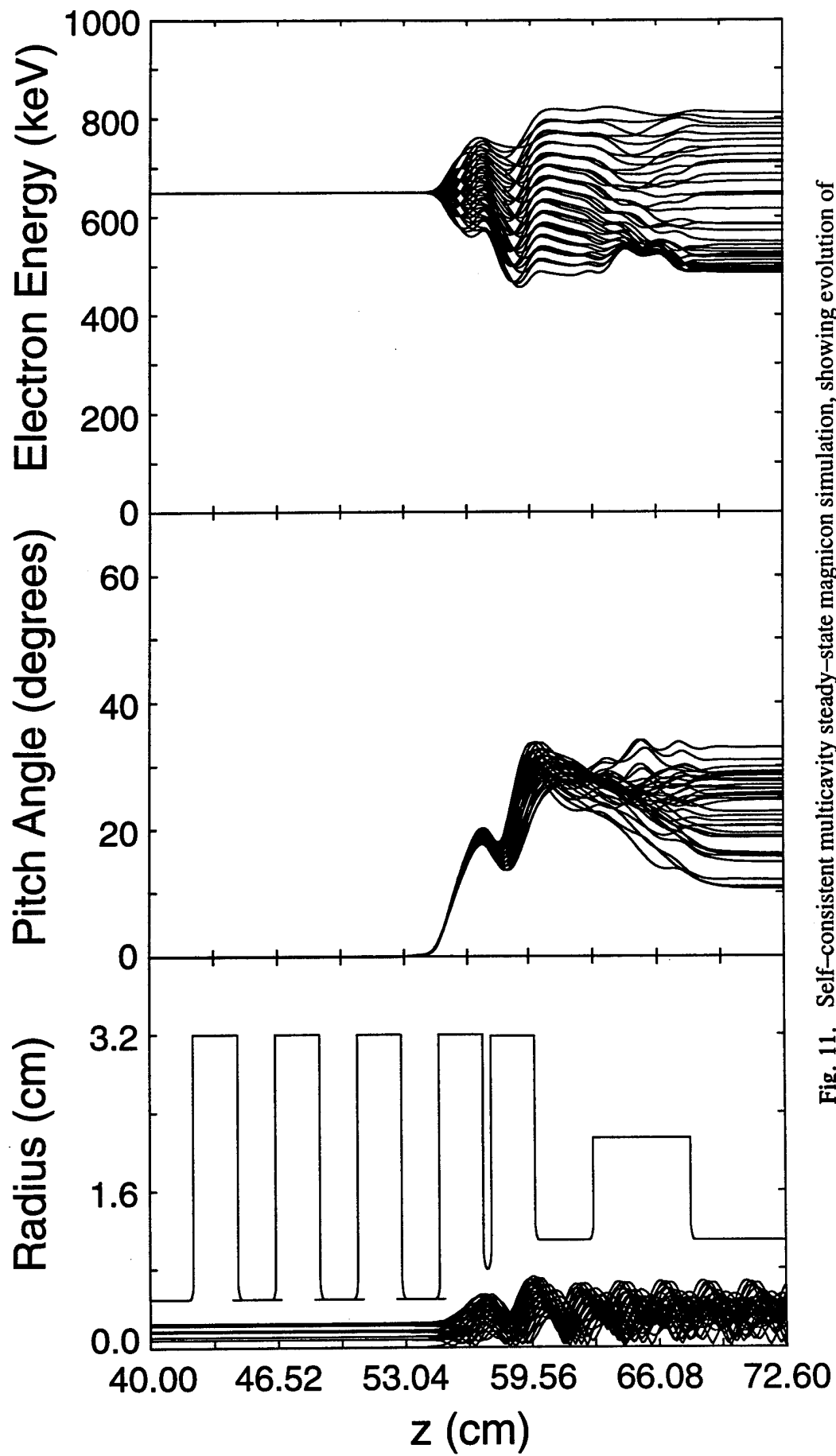


Fig. 11. Self-consistent multicavity steady-state magnicon simulation, showing evolution of beam trajectories, energy, and pitch angle for $B_z=7.2$ kG and $H_{rf}=55$ kA/m. There are no rf fields in the first three deflection cavities.